Journal of Cerebral Blood Flow & Metabolism (2014) 34, 1818–1825

www.jcbfm.com

ORIGINAL ARTICLE

Kinetic modeling of ^{11}C-LY2795050, a novel antagonist radiotracer for PET imaging of the kappa opioid receptor in humans

Mika Naganawa[1], Ming-Qiang Zheng[1], Nabeel Nabulsi[1], Giampaolo Tomasi[1], Shannan Henry[1], Shu-Fei Lin[1], Jim Ropchan[1], David Labaree[1], Johannes Tauscher[2], Alexander Neumeister[3], Richard E Carson[1] and Yiyun Huang[1]

^{11}C-LY2795050 is a novel kappa opioid receptor (KOR) antagonist tracer for positron emission tomography (PET) imaging. The purpose of this first-in-human study was to determine the optimal kinetic model for analysis of ^{11}C-LY2795050 imaging data. Sixteen subjects underwent baseline scans and blocking scans after oral naltrexone. Compartmental modeling and multilinear analysis-1 (MA1) were applied using the arterial input functions. Two-tissue compartment model and MA1 were found to be the best models to provide reliable measures of binding parameters. The rank order of ^{11}C-LY2795050 distribution volume (V_T) matched the known regional KOR densities in the human brain. Blocking scans with naltrexone indicated no ideal reference region for ^{11}C-LY2795050. Three methods for calculation of the nondisplaceable distribution volume (V_{ND}) were assessed: (1) individual V_{ND} estimated from naltrexone occupancy plots, (2) mean V_{ND} across subjects, and (3) a fixed fraction of cerebellum V_T. Approach (3) produced the lowest intersubject variability in the calculation of binding potentials (BP_{ND}, BP_F, and BP_P). Therefore, binding potentials of ^{11}C-LY2795050 can be determined if the specific binding fraction in the cerebellum is presumed to be unchanged by diseases and experimental conditions. In conclusion, results from the present study show the suitability of ^{11}C-LY2795050 to image and quantify KOR in humans.

Journal of Cerebral Blood Flow & Metabolism (2014) **34,** 1818–1825; doi:10.1038/jcbfm.2014.150; published online 3 September 2014

Keywords: brain imaging; kinetic modeling; positron emission tomography; receptors; receptor imaging

INTRODUCTION

The kappa opioid receptor (KOR) is one of the three major subtypes of opioid receptors. The distribution of KOR in human brain has been investigated *in vitro* with autoradiography, or radioligand binding assays using homogenized brain tissue.[1–4] Kappa opioid receptor exists abundantly in amygdala, anterior cingulate cortex and insula, with moderate levels in the neocortical regions and putamen, followed by caudate, thalamus, globus pallidus, hippocampus, pons, and substantia nigra. Using reverse transcription-PCR detection of human KOR transcripts in human brain,[5] a signal was detected in most regions including the cerebellum. A low density of KOR was observed in cortex white matter by autoradiography using ^{3}H-U69593.[4]

Multiple lines of evidence from preclinical and clinical studies have implicated KOR in a variety of neuropsychiatric disorders, including substance abuse,[6,7] epilepsy,[8,9] Alzheimer's disease[10,11] and major depression.[12–14] As a result, considerable efforts have been made to develop radiotracers to image KOR in humans and probe its involvement in the pathophysiology of these disorders. A number of ligands have been developed, including ^{11}C-GR103545,[15] ^{11}C-MeJDTic[16] and ^{11}C-LY2795050.[17] ^{11}C-GR103545 is an agonist tracer extensively evaluated in nonhuman primates,[18–20] and recently in humans.[21] However, KOR agonists at relatively low mass doses elicit dysphoric[22] and psychomimetic[14] effects. Therefore, the use of agonist radiotracers in human positron emission tomography (PET) imaging requires careful control of the injected mass. On the other hand, KOR antagonists have been targeted for development as potential pharmacological agents for the treatment of a wide range of conditions such as drug addiction, depression, and feeding behavior,[23] and the application of antagonist radiotracers will make it possible to more easily perform KOR imaging in human. For antagonist tracers, ^{11}C-MeJDTic had high KOR affinity ($K_i = 1.01 \pm 0.17$ nmol/L; human cloned KOR)[24] and was evaluated in mice,[16] but no reports of its use in nonhuman primates or humans have been published. We have recently developed ^{11}C-LY2795050 ($K_i = 0.72$ nmol/L; human cloned KOR)[17] as a novel, KOR-selective antagonist radiotracer and showed its suitability to image KOR in rhesus monkey.[17,25] The *in vitro* selectivity for KOR over mu or delta opioid receptor was estimated to be 35.8 and 212.5 times, respectively.[17] The affinity of LY2795050 for the opioid receptors was measured by radioligand displacement experiments with cloned human opioid receptors and the opioid antagonist radioligand ^{3}H-diprenorphine, and naltrexone was used to define nonspecific binding.[26]

[1]Department of Diagnostic Radiology, PET Center, Yale University School of Medicine, New Haven, Connecticut, USA; [2]Eli Lilly and Company, Indianapolis, Indiana, USA and [3]Department of Psychiatry and Radiology, New York University School of Medicine, New York, New York, USA. Correspondence: Dr M Naganawa, Department of Diagnostic Radiology, PET Center, Yale University School of Medicine, PO Box 208048, New Haven, CT 06520-8048, USA.
E-mail: mika.naganawa@yale.edu
This study was supported by Eli Lilly and Company, and by a research grant from NIMH (1 R01 MH091537 to YH). This publication was also made possible by CTSA Grant UL1 RR024139 from the National Center for Research Resources (NCRR) and the National Center for Advancing Translational Sciences (NCATS), components of the National Institutes of Health (NIH). Its contents are solely the responsibility of the authors and do not necessarily represent the official view of NIH.
Received 15 May 2014; revised 15 July 2014; accepted 31 July 2014; published online 3 September 2014

In this paper, we present the results from our first-in-human study with the selective KOR antagonist ^{11}C-LY2795050. Our goals are (1) to determine the appropriate model to describe its *in vivo* kinetics and (2) to choose a suitable method to define the nondisplaceable distribution volume (V_{ND}) for derivation of binding potentials.

MATERIALS AND METHODS

Human Subjects

Sixteen healthy subjects (24 to 56 years of age; 8 men and 8 women, body weight 75 ± 10 kg) were included. Studies were performed under protocols approved by the Yale University School of Medicine Human Investigation Committee and the Yale-New Haven Hospital Radiation Safety Committee, and in accordance with the United States federal guidelines and regulations for the protection of human research subjects contained in Title 45 Part 46 of the Code of Federal Regulations (45 CFR 46). Written informed consent was obtained from all subjects. As part of the subject evaluation, magnetic resonance (MR) images were acquired on all subjects to eliminate those with structural brain abnormalities and for PET image registration. The MR imaging was performed on a 3-T whole-body scanner (Trio, Siemens Medical Systems, Erlangen, Germany) with a circularly polarized head coil. The dimension and pixel size of MR images were $256 \times 256 \times 176$ and $0.98 \times 0.98 \times 1.0\,mm^3$, respectively.

Radiotracer Synthesis

^{11}C-LY2795050 was synthesized as previously described.[17] Radiochemical purity of ^{11}C-LY2795050 in the final product solution was $>99\%$.

Positron Emission Tomography Imaging Experiments

Subjects underwent two PET scans on the same day: a baseline ^{11}C-LY2795050 PET scan followed by a second scan at ~75 minutes after an oral administration of 150 mg naltrexone, a nonselective opioid receptor antagonist. The time between tracer injections was 4.8 ± 0.9 hours. For one subject with ^{11}C-LY2795050, baseline and blocking scans were performed 1 month apart.

Positron emission tomography scans were conducted on the High Resolution Research Tomograph (HRRT) (Siemens Medical Solutions, Knoxville, TN, USA), which acquires 207 slices (1.2 mm slice separation) with a reconstructed image resolution (full width at half maximum) of ~3 mm. Before tracer administration, a 6-minute transmission scan was conducted for attenuation correction. Each scan was acquired in list mode for 90 minutes after intravenous administration of tracer over 1 minute by an automatic pump (Harvard PHD 22/2000; Harvard Apparatus, Holliston, MA, USA). The injected mass limit was 10 μg. Dynamic scan data were reconstructed in 27 frames (6×0.5 minutes, 3×1 minutes, 2×2 minutes, 16×5 minutes) with corrections for attenuation, normalization, scatter, randoms, and deadtime using the MOLAR algorithm.[27] Event-by-event motion correction[28] was included in the reconstruction based on measurements with the Polaris Vicra sensor (NDI Systems, Waterloo, Canada) with reflectors mounted on a swim cap worn by the subject.

Input Function Measurement

For each subject, the radial artery was catheterized for blood sampling. An automated blood counting system (PBS-101; Veenstra Instruments, Joure, The Netherlands) was used to measure the radioactivity in whole blood during the first 7 minutes. Thirteen samples (2 to 10 mL) were collected manually at selected time points after tracer administration starting at 3 minutes. For each sample, plasma was obtained by centrifugation at 4°C (2,930 *g* for 5 minutes). Whole blood and plasma were counted in crosscalibrated gamma counters (1480 & 2480 WIZARD; Perkin-Elmer, Waltham, MA, USA).

To determine radioactivity in plasma for the first 7 minutes, the whole blood-to-plasma ratios were calculated from the hand-drawn samples. The ratio from 3 to 90 minutes was fitted to the following equation: $at+b$, and the plasma time-activity curve (TAC) in the first 7 minutes was calculated from the measured whole blood TAC and the extrapolated ratio. These data were combined with those from the plasma samples to produce the final curve of total radioactivity in plasma. To reduce noise in these data, the total plasma curve from ~5 minutes onward was fitted to a sum of exponentials.

Plasma Metabolite Analysis

Analysis of the metabolite profile in the arterial plasma was performed using a modified automatic column-switching HPLC method.[29] Plasma samples collected at 5, 15, 30, 60, and 90 minutes after injection were mixed with urea (8 mol/L) and then filtered through 1.0 μm Whatman 13 mm GD/X syringe filters (GE, Florham Park, NJ, USA). Up to 5 mL of plasma filtrate was injected to the automatic HPLC system equipped with a Gemini-NX analytical column (4.6 × 250 mm, 5 μm; Phenomenex, Torrance, CA, USA) and eluted with a mobile phase consisting of 45% acetonitrile and 55% 0.1 mol/L ammonium formate (v/v) at a flow rate of 1.5 mL/min. The HPLC eluate was fraction-collected and counted in the gamma counters. The fraction counts were corrected for volume and decay. The unmetabolized parent fraction was calculated as the ratio of the sum of radioactivity in fractions containing the parent compound to the total amount of radioactivity collected, and fitted to an integrated gamma function (four fitted parameters: *a*, *b*, *c*, and *d*):

$$f(t) = a \times \left(1 - b\int_0^{ct} \exp(-u)u^{d-1}du \Big/ \int_0^{\infty} \exp(-u)u^{d-1}du\right) \quad (1)$$

In addition, the time-varying extraction efficiency of radioactivity in filtered plasma samples was determined, and normalized to that of reference plasma sample. The plasma input function was calculated as the product of the total plasma activity, the parent HPLC fraction, and the normalized extraction efficiency.

Measurement of Tracer-Free Fraction in Plasma

Arterial blood samples were taken immediately before tracer injection for analysis of plasma-free fraction (f_P). An ultrafiltration (Millipore Centrifree micropartition device, 4104, Billerica, MA, USA) method was used for measuring f_P of tracer in plasma in triplicate. The free fraction f_P was determined from the count ratio of ultrafiltrate to plasma.

Image Registration and Definition of Regions of Interest

Regions of interest (ROIs) were taken from the AAL (Automated Anatomical Labeling) for SPM2[30] in MNI (Montreal Neurological Institute) space.[31] For each subject, the dynamic PET images after hardware motion correction were coregistered to the early summed PET images (0 to 10 minutes after injection) using a 6-parameter mutual information algorithm[32] (FLIRT of FSL) to eliminate any residual motion. The summed PET image was then coregistered to the subject's T1-weighted 3 T MR image (6-parameter rigid registration), which was subsequently coregistered to the AAL template in MNI space using a nonlinear transformation (Bioimage suite).[33] Using the combined transformations from template to PET space, regional TACs were generated for 14 ROIs: amygdala, caudate, centrum semiovale, cerebellum, anterior cingulate cortex, posterior cingulate cortex, frontal lobe, globus pallidus, hippocampus, insula, occipital lobe, putamen, temporal lobe, and thalamus.

Quantitative Analysis

Outcome measures were derived with kinetic analysis of the regional TACs using the arterial plasma TAC as an input function. The distribution volume (V_T)[34] was calculated using one- and two-tissue compartment models (1TC and 2TC), as well as the multilinear analysis-1 (MA1) method.[35] The time stability of V_T estimates was evaluated by fitting the model to regional TACs with shortened scan durations, ranging from 90 to 30 minutes for 2TC, and from 90 to 50 minutes for MA1 ($t^* = 30$ minutes) model. The ratio of V_T value from the shortened scan to that from the 120-minute scan was computed for each ROI and duration. The following two criteria were used to determine a minimum scan duration[36]: (a) the average of the ratio was between 0.95 and 1.05; and (b) the interindividual standard deviation of the ratio was <0.1. The nondisplaceable distribution volume (V_{ND}) required for computing binding potentials was calculated from the occupancy plots (see below). The simplified reference tissue model (SRTM) with the cerebellum as a reference region was also applied to the regional TACs. Due to the lack of a suitable reference region, the estimated binding potential (BP_{ND}) values were corrected (see below). All modeling was performed with in-house programs written with IDL 8.0 (ITT Visual Information Solutions, Boulder, CO, USA). For parameter estimation, data points were weighted based on noise equivalent counts in each frame. Percentage standard error (%s.e.) was estimated from the theoretical parameter covariance matrix.

The KOR occupancy (r) by naltrexone and nondisplaceable distribution volume (V_{ND}) were calculated from the following equation:[37]

$$V_T(\text{baseline}) - V_T(\text{blocking}) = r(V_T(\text{baseline}) - V_{ND}). \quad (2)$$

For each subject, the percentage of specific binding was calculated as the difference between V_T and V_{ND} divided by V_T. All regions were used for the occupancy plots in the naltrexone blocking study, assuming uniform KOR occupancy. On the basis of the estimated V_{ND}, the three binding potentials, BP_{ND}, BP_P and BP_F were calculated using MA1-based V_T estimates. The value of V_{ND} was calculated in three ways: (1) individual V_{ND} from each occupancy plot, (2) the mean V_{ND} from all occupancy plots (i.e., a constant value for all subjects), and (3) the fraction of cerebellum V_T corresponding to nonspecific binding. Approach (3) was used for both MA1 and SRTM models. Assuming that $V_{T\ CER} = \alpha V_{ND}$ (α is a constant value) in the pseudo reference tissue model,[38] the corrected BP_{ND} is described as $\alpha(BP_{ND}+1) - 1$. The fraction value α was determined as the average ratio of the cerebellum V_T to the V_{ND} estimated from individual occupancy plots used in method (1).

RESULTS

Injection Parameters

In the baseline and blocking scans, the subjects received radioactivity doses of 334 ± 149 MBq and 334 ± 152 MBq, respectively, with specific activity of 14.8 ± 6.5 GBq/μmol and 16.2 ± 6.8 GBq/μmol at the time of injection. Injections were performed by computer-controlled syringe pump. Injected mass was $9.3 \pm 0.9\ \mu$g and $8.7 \pm 2.1\ \mu$g for baseline and blocking scans, respectively. In most cases, the mass limit of $10\ \mu$g was the limiting factor, thus there was very little variability in the magnitude of injected mass.

Plasma Analysis

In either the baseline or blocking scan, total plasma activity stabilized at a constant level after 20 minutes after injection (Figure 1A). ^{11}C-LY2795050 metabolized fairly quickly in plasma (Figure 1B), with the parent fraction decreasing to $44 \pm 8\%$ and $18 \pm 5\%$, respectively, at 30 and 90 minutes after injection in the baseline scans ($n = 16$). The parent fractions in the naltrexone blocking scans were similar to those from the baseline scans (Figure 1B). The estimated metabolite-corrected radioactivity time course in the arterial plasma is shown in Figure 1C. The plasma-free fraction (f_P) of ^{11}C-LY2795050 was $0.77 \pm 0.16\%$ for baseline scans ($n = 16$) and $0.75 \pm 0.16\%$ for blocking scans ($n = 16$).

Brain Uptake and Kinetics

Uptake images from the baseline and naltrexone-blocking scans are shown in Figure 2. Regional TACs for representative brain regions are shown in Figure 3. ^{11}C-LY2795050 displayed favorable imaging properties in the brain, with rapid entry, heterogeneous regional accumulation and fast kinetics. Activity peaked at ~4 minutes in all brain regions (Figures 3A and 3B). Pretreatment with naltrexone reduced the uptake of the radiotracer in all brain regions, suggesting specific binding of the radiotracer in the brain (Figures 2C, 3C, and 3D), given the lack of change in the input function (Figure 1C).

Kinetic Model Assessment

The baseline scans were used to assess the best model for kinetic analysis. The 1TC and 2TC models reached convergence for every scan in all regions. The mean value of K_1 in the 1TC model ranged from 0.04 mL/cm^3 per minute in the centrum semiovale to 0.11 mL/cm^3 per minute in the occipital cortex. The k_4 value ranged from 0.025 ± 0.003/min (centrum semiovale) to 0.054 ± 0.038/min (cerebellum). The thalamus showed a high k_4 value (0.085 ± 0.031/min).

The 2TC model was favored over the 1TC model according to the AIC and visual assessment of the quality of fits (Figures 3A and 3C). The F test indicated a significantly better fit for the 2TC model in 223 out of 224 regions. In two cases, the 2TC model provided moderately large V_T estimate with large %s.e. ($> 10\%$) in the posterior cingulate. Due to the lack of fit with 1TC model and the variability in 2TC V_T estimates, the MA1 model was also evaluated. While the V_T values derived from the 1TC model were slightly lower than those from the 2TC model ($V_{T\ (1TC)} = 0.94\ V_{T\ (2TC)} - 0.09$, $R^2 = 0.96$), the V_T values from MA1 matched extremely well with those from the 2TC model ($V_{T\ (MA1,\ t^* = 30\ min)} = 0.98\ V_{T\ (2TC)} + 0.06$, $R^2 = 0.98$) (Supplementary Figure S1). The setting for t^* in MA1 had almost no effect on V_T estimates (Supplementary Figure S2) for $t^* \geq 30$ minutes. Note that these comparisons were conducted for the regions with good identifiability, i.e., %s.e. of $V_T < 10\%$ with the 2TC model.

The V_T values derived from 1TC, 2TC, and MA1 model and the minimum scan time for 2TC and MA1 models are shown in Table 1. High V_T values were seen in amygdala, insula, and anterior cingulate cortex. Intermediate V_T values were found in globus pallidus, putamen, temporal cortex, frontal cortex, and occipital cortex. Lower V_T values were in hippocampus, caudate, posterior cingulate cortex, thalamus, and centrum semiovale, with the lowest V_T value in the cerebellum. The intersubject V_T variability was low in all models (average of %COV = 10 to 12%). The minimum scan duration was 70 minutes to satisfy all stability criteria in all regions for both 2TC and MA1 models (Table 1).

Blocking of Specific Binding by Naltrexone

In all regions, the V_T values displayed statistically significant reduction in blocking scans after oral naltrexone ($P < 0.00001$) (Table 1), i.e., no region was found that would serve as a reference region. As determined from the occupancy plots (Figure 4), 150 mg of oral naltrexone occupied $93 \pm 6\%$ of specific binding. The nondisplaceable distribution volume (V_{ND}) for ^{11}C-LY2795050 was estimated as 1.61 ± 0.25 mL/cm^3 (range: 1.13 to 2.06 mL/cm^3).

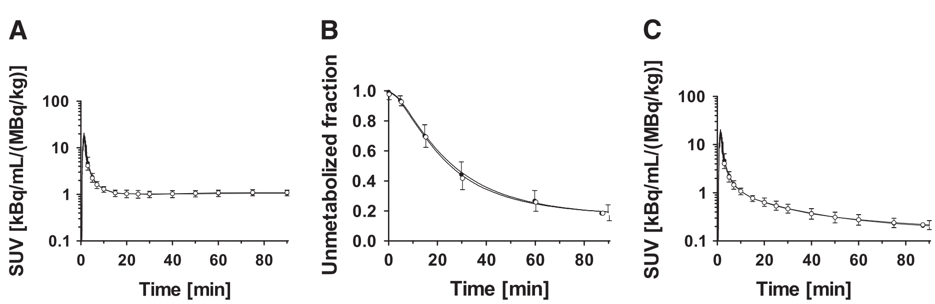

Figure 1. Mean ± s.d. of (**A**) total plasma activity, (**B**) parent fraction in the plasma, and (**C**) metabolite-corrected plasma activity over time after injection of ^{11}C-LY2795050 in the baseline (closed circles, $n = 16$) and blocking (open circles, $n = 16$) scans. (**A**) and (**C**) Displayed in SUV units (concentration/(injected dose/body weight)). SUV, standard uptake value.

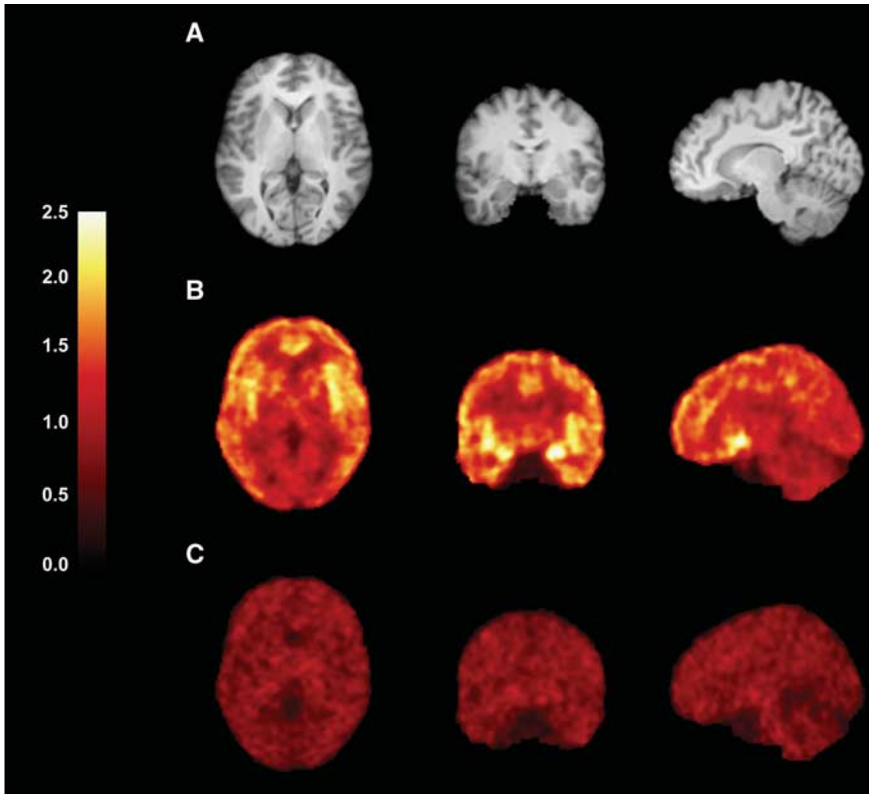

Figure 2. Images from a typical subject (female, 32 years old, 77 kg body weight). (**A**) Magnetic resonance (MR) images. (**B** and **C**) Coregistered positron emission tomography (PET) images summed from 30 to 90 minutes after injection of ^{11}C-LY2795050. (**B**) Baseline scan and (**C**) postnaltrexone scan. Activity is expressed as SUV (concentration/(injected dose/body weight)). PET images were spatially smoothed by three-dimensional Gaussian filter with full width at half maximum (FWHM) (3.6 mm). SUV, standard uptake value.

V_{ND} or occupancy values did not have any significant correlation with either gender or subject weight.

The specific binding percentage in the cerebellum ($=(V_{T\ CER\ (baseline)} - V_{ND})/V_{T\ CER(baseline)}$), the region with the lowest V_T, was estimated at $17 \pm 10\%$ (range: 4 to 38%), suggesting that cerebellar V_T might be a useful estimator of V_{ND}, if corrected. The slope and intercept of the regression line of V_{ND} estimates against cerebellum V_T were 1.00 ± 0.29 (95% confidence interval: 0.37 to 1.6) and -0.34 ± 0.57 (−2.4 to 0.97), respectively. Thus, the intercept was not significantly different from 0 ($P = 0.57$), and the slope was not significantly different from 1/1.17 ($P = 0.63$). Thus, we evaluated three approaches to define V_{ND} to calculate binding potentials: (1) individual V_{ND} from the occupancy plot, (2) mean V_{ND} across subjects from the occupancy plots (1.61 mL/cm^3), and (3) a fixed fraction of each individual's cerebellum V_T ($V_{T\ CER\ (baseline)}$/1.17). Among these three ways to estimate V_{ND}, method (3) provided the lowest intersubject variability in all binding potentials (BP_{ND}, BP_P, and BP_F). The binding potential values from MA1 and SRTM with method (3) are summarized in Table 2. In method (3), the intersubject variability was smallest in BP_{ND} (mean across regions: 22%), followed by BP_P (23%), and BP_F (30%). For method (2), using the average V_{ND}, variability was substantially higher: BP_{ND} (32%), BP_P (32%), and BP_F (36%). Using individual V_{ND} values in method (1) produced the highest intersubject variability: BP_{ND} (39%), BP_P (28%), and BP_F (35%). The corrected BP_{ND} values derived from SRTM were lower than those from the MA1 model (corrected $BP_{ND\ (SRTM)} = 0.89 \times$ corrected $BP_{ND\ (MA1)} + 0.06$, $R^2 = 0.98$).

In Vivo Affinity of ^{11}C-LY2795050

The *in vivo* BP_F values from the present study were correlated with unweighted averages of previously reported regional KOR concentrations (B_{max}) obtained *in vitro* from ligand competition binding assays in brain tissue homogenates or autoradiography studies using radioligand ^{3}H-diprenorphine,[1] ^{3}H-etrophine,[2,3] or ^{3}H-ethylketocyclazocine[3] in the presence of different displacing agents or ^{3}H-U69593.[4] In the *in vitro* literature, the unit of specific binding is fmol/mg protein. This unit can be converted to fmol/mg of wet tissue by assuming that there is ~0.1 mg protein per mg of wet tissue.[39] A correlation plot of the regional binding potential $BP_F(= B_{avail}/K_D)$ and the *in vitro* B_{max} is shown in Figure 5. A statistically significant correlation was found with the regression equation of $B_{max} = 0.028 \times BP_F$ ($R^2 = 0.20$, $P < 0.0001$, $n = 10$). Since $BP_F = B_{max}/K_D$, the slope of this regression line represents the *in vivo* K_D of ^{11}C-LY2795050. We also correlated the *in vivo* BP_F values with *in vitro* B_{max} values obtained from the individual studies that contributed to the average B_{max} values used above. The K_D estimates ranged from 0.019 nmol/L (^{3}H-diprenorphine, $R^2 = 0.43$, $P < 0.0001$, $n = 9$) to 0.056 nmol/L (^{3}H-etrophine by Cross *et al*, $R^2 = 0.61$, $P < 0.05$, $n = 3$) (Supplementary Figure S3). In the analysis, the determination coefficient was very low ($R^2 < 0.1$) with *in vitro* B_{max} if amygdala, putamen, and globus pallidus measured by ^{3}H-etrophine are included. Thus, these three regions were excluded from the comparison when using ^{3}H-etrophine data.

Receptor occupancy by the carrier mass of LY2795050 was calculated by $100 \times F/(F + K_D)$, where F is the mean value (from 60 to 90 minutes after injection) of the metabolite-corrected and protein-unbound plasma concentration (expressed in nmol/L), and *in vivo* K_D is assumed to be 0.028 nmol/L (estimated in this study). In all scans, the occupancy by LY2795050 was $< 5\%$. Receptor occupancy estimated using the *in vitro* K_i (0.72 nmol/L) of LY2795050 was even lower.

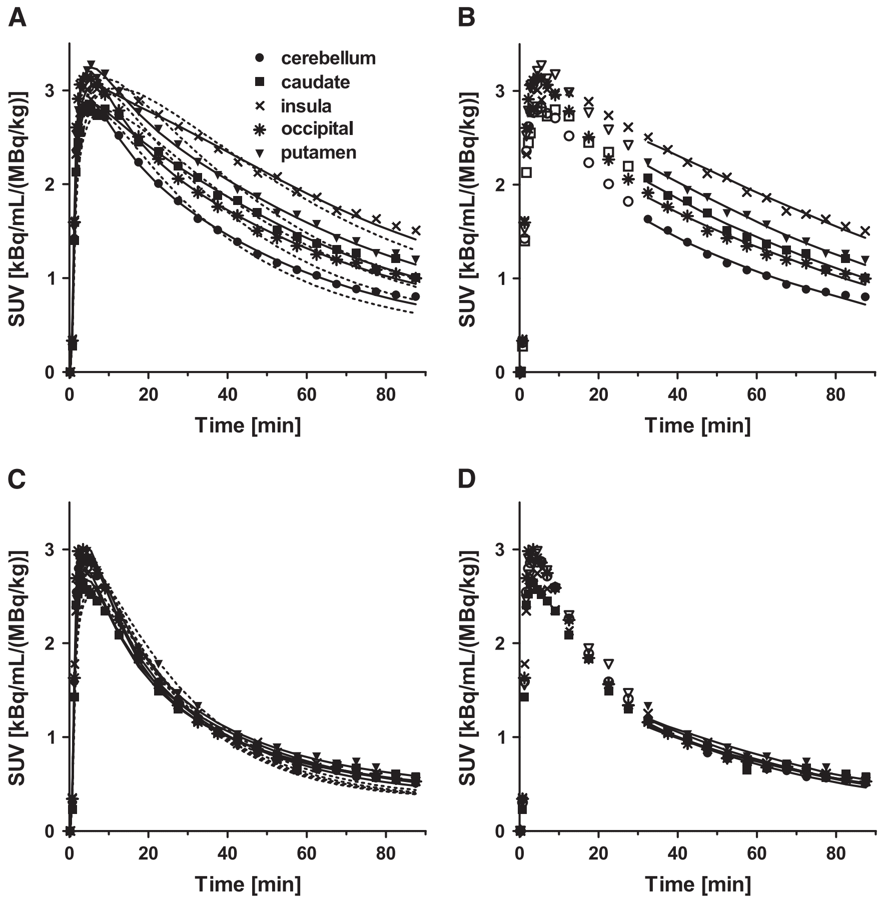

Figure 3. Regional time-activity curves in five regions of interest (ROIs) after injection of ^{11}C-LY2795050 from the baseline (**A** and **B**) and naltrexone blocking (**C** and **D**) scans. Panels **A** and **C** display the 1TC (dotted line) and 2TC (solid line) fits and panels **B** and **D** display the MA1 fits. For each region, the symbols correspond to the measured regional activity.

Table 1. Regional distribution volumes of ^{11}C-LY2795050 in baseline and blocking scans

Regions	*Baseline* (n = 16)			*Blocking with naltrexone* (n = 16)	*Minimum scan duration (minutes)*	
	1TC (%COV)	*2TC (%COV)*	*MA1 (%COV)*	*MA1 (%COV)*	*2TC*	*MA1*
Amygdala	3.76 (13%)	3.95 (13%)	3.95 (14%)	1.62 (15%)	60	70
Insula	3.09 (9%)	3.41 (10%)	3.41 (10%)	1.68 (14%)	70	50
Ant. cingulate cortex	2.98 (10%)	3.23 (11%)	3.25 (10%)	1.71 (13%)	60	50
Globus pallidus	2.86 (11%)	3.11 (12%)	3.11 (12%)	1.90 (14%)	50	60
Putamen	2.65 (10%)	3.00 (11%)	2.94 (10%)	1.81 (14%)	70	50
Temporal cortex	2.44 (9%)	2.74 (11%)	2.71 (10%)	1.70 (13%)	70	60
Frontal cortex	2.34 (9%)	2.66 (11%)	2.63 (10%)	1.64 (14%)	70	50
Occipital cortex	2.24 (8%)	2.58 (10%)	2.54 (9%)	1.77 (12%)	70	60
Hippocampus	2.07 (11%)	2.31 (12%)	2.35 (12%)	1.58 (14%)	60	50
Caudate	1.99 (16%)	2.19 (17%)	2.16 (16%)	1.40 (19%)	60	50
Post. cingulate cortex	1.93 (13%)	2.24 (17%)	2.24 (12%)	1.61 (13%)	70	60
Thalamus	2.03 (10%)	2.14 (10%)	2.18 (11%)	1.78 (14%)	30	50
Centrum semiovale	1.90 (8%)	2.30 (10%)	2.28 (10%)	1.86 (15%)	70	70
Cerebellum	1.76 (8%)	1.96 (9%)	1.95 (8%)	1.57 (13%)	70	50

MA1, multilinear analysis-1; 1TC, one-tissue compartment model; 2TC, two-tissue compartment model. %COV is variability across subjects.

DISCUSSION

In this study, we conducted the first-in-human evaluation with the selective KOR antagonist ^{11}C-LY2795050. Our goals were (1) to determine the optimal model to describe its kinetics, (2) to assess the specific binding component from blocking study with 150 mg of oral naltrexone, and (3) to determine an appropriate method to estimate the nondisplaceable volume of distribution from the blocking data.

The metabolism profile of ^{11}C-LY2795050 in human (44% parent fraction at 30 minutes) was similar to that of rhesus monkey (40% parent fraction at 30 minutes).[17] Similar to the monkey study, ^{11}C-LY2795050 readily entered into the human brain, and was washed out rapidly (Figure 3). The radioactivity in the brain reached peak levels at ~4 minutes after injection. This suggests that ^{11}C-LY2795050 has favorable properties as a radiotracer. The rank order of uptake was also similar to that in the rhesus monkey and consistent with regional KOR densities measured in human postmortem studies *in vitro* (Figure 5).

The 2TC model[17] and MA1 model with $t^* = 40$ minutes[25] were used as the models of choice for analysis of ^{11}C-LY2795050 imaging data in rhesus monkeys, with 2TC providing better fits than 1TC. This was also true in humans. The MA1 V_T values matched extremely well with those from 2TC. Thus, the 2TC model and MA1 model were selected as suitable models to describe ^{11}C-LY2795050 kinetics in the human brain. In addition, the t^* setting did not have a strong effect on V_T estimates (Supplementary Figure S2). While a late t^* value (e.g., 60 minutes) would produce unstable V_T estimates due to a smaller number of data points for fitting, MA1 analysis with $t^* = 30$, 40, or 50 minutes all produced reliable V_T estimates. One caveat is that the 2TC model in the present human study produced V_T estimates with a large standard error in a few cases. Higher levels of noise are usually found in human imaging data compared with those in nonhuman primates, so larger errors in the model parameters are expected. The MA1 model would be more suitable for parametric imaging due to a reasonable computation time. Additional data from more subjects would help with the evaluation of an optimal model for analysis.

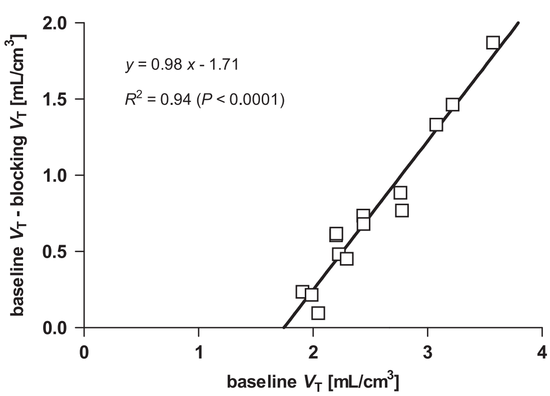

Figure 4. A typical occupancy plot of ^{11}C-LY2795050 using V_T in all regions of interest (ROIs) from the baseline and blocking scans (150 mg naltrexone). Occupancy is measured as the slope of the regression line, and ^{11}C-LY2795050 V_{ND} is the x-axis intercept.

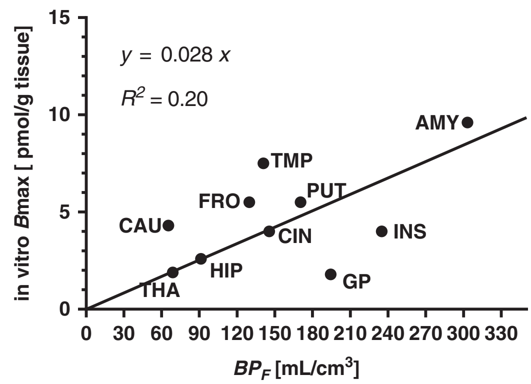

Figure 5. Correlations between regional BP_F estimates of ^{11}C-LY2795050 and kappa receptor B_{max} values measured *in vitro*. *In vitro* B_{max} values were the unweighted averages as measured in autoradiography studies with the radioligand ^{3}H-diprenorphine (Pfeiffer *et al*[1]), ^{3}H-etrophine (Delay-Goet *et al*[3] and Cross *et al*[2]), ^{3}H-U69593 (Barg *et al*[4]), or ^{3}H-ethylketocyclazocine with various displacing agents (Delay-Goet *et al*[3]). Ten regions of interest (ROIs) were used to compare *in vivo* data with *in vitro* measurements of kappa opioid receptor (KOR) B_{max}: amygdala (AMY), insula (INS), temporal cortex (TMP), frontal cortex (FRO), globus pallidus (GP), putamen (PUT), caudate (CAU), cingulate cortex (CIN), hippocampus (HIP), and thalamus (THA). For the cingulate cortex, BP_F values were computed as the unweighted average between anterior and posterior cingulates. The regression equation was derived as $B_{max} = 0.028 \times BP_F$ ($R^2 = 0.20$). BP, binding potential.

Table 2. Regional binding potential values of ^{11}C-LY2795050 from SRTM and MA1

Regions	*Baseline* (n = 16)			
	SRTM	*MA1*		
	BP_{ND} (%COV)	BP_{ND} (%COV)	BP_P (%COV)	BP_F (%COV)
Amygdala	1.28 (18%)	1.37 (19%)	2.29 (21%)	303.09 (23%)
Insula	1.00 (11%)	1.05 (11%)	1.75 (14%)	234.97 (22%)
Ant. cingulate cortex	0.91 (18%)	0.96 (18%)	1.59 (17%)	212.65 (24%)
Globus pallidus	0.84 (16%)	0.87 (17%)	1.45 (19%)	194.38 (25%)
Putamen	0.75 (15%)	0.77 (15%)	1.28 (16%)	170.54 (21%)
Temporal cortex	0.61 (15%)	0.63 (15%)	1.05 (17%)	140.97 (23%)
Frontal cortex	0.57 (17%)	0.59 (18%)	0.97 (18%)	129.71 (24%)
Occipital cortex	0.57 (19%)	0.53 (14%)	0.88 (16%)	117.22 (22%)
Hippocampus	0.45 (21%)	0.42 (28%)	0.69 (29%)	91.33 (32%)
Caudate	0.29 (58%)	0.30 (57%)	0.50 (57%)	65.37 (61%)
Post. cingulate cortex	0.45 (30%)[a]	0.36 (43%)	0.58 (42%)	78.61 (51%)
Thalamus	0.40 (23%)	0.37 (21%)	0.52 (31%)	68.87 (34%)
Centrum semiovale	0.33 (29%)	0.32 (32%)	0.62 (22%)	82.65 (28%)
Cerebellum		0.17 (0%)	0.29 (8%)	39.24 (23%)

BP, binding potential; MA1, multilinear analysis-1; SRTM, simplified reference tissue model. %COV is variability across subjects. V_{ND} was assumed to be 85% of the distribution volume in the cerebellum. [a]The values with %s.e. > 100% were excluded ($n = 10$).

Given the low *in vivo* K_D estimate (0.028 nmol/L), small k_4 values with the 2TC model are possible. For ^{11}C-LY2795050, the average k_4 value across all regions was 0.046 ± 0.015/min. The value was similar to the estimates from ^{11}C-FLB 457 (k_4: $0.02 \sim 0.05$/min),[40] which also has a high affinity to D_2/D_3 receptors (0.02 nmol/L). Note that the instability of k_4 estimation should be considered when discussing a relationship between K_D and k_4 values.

The centrum semiovale was included in the occupancy plot measurements since its V_T was decreased by naltrexone blocking. This blockade was consistent with *in vitro* data; in the autoradiography study using ^{3}H-U69593, low density of KOR was detected in the white matter. The occupancy plot relies on the assumption that V_{ND} is the same in all included regions, which could be different in white matter, but in retrospect, the centrum semiovale was not an outlier on occupancy plots. Occupancy and V_{ND} values from the occupancy plots without the centrum semiovale were only $2 \pm 1\%$ lower than those with the centrum semiovale included.

In the rhesus monkey study with ^{11}C-LY2795050, the cerebellum was found to be a suitable reference region, since there was no difference between V_T values at baseline and following varying blocking doses of LY2795050. On the other hand, V_T values in the present study with naltrexone blocking were significantly reduced in all regions, indicating the lack of an ideal reference region for ^{11}C-LY2795050 in humans. Therefore, we assessed three methods for the determination of V_{ND}, using intersubject variability of the resulting BP_{ND}, BP_P, and BP_F as an evaluation and selection criterion.

For all binding potentials, the lowest variability was seen when V_{ND} was estimated as a fraction of the cerebellar V_T (method (3)). This suggests that the estimated cerebellum V_T correlates with V_T estimates for other regions, and therefore the use of the corrected cerebellar V_T value as V_{ND} reduces intersubject variability by cancellation of common error or variability. When binding potentials were estimated using individual V_{ND} values derived from occupancy plot of individual subjects (method (1)), high variability in the estimates was found. This is because individual V_{ND} had higher intersubject variability (%COV = 15%) than the fractional cerebellum V_T (%COV = 8%). Individual V_{ND} was determined as the *x*-axis intercept of the occupancy plot (Figure 4), which is often associated with larger estimation error compared with slope estimation. Interestingly, using the mean V_{ND} (constant value for all subjects, method (2)) yielded binding potential variability that was intermediate between methods (1) and (3), which either suggests that there is true intersubject variability in V_{ND}, or that the cancellation of inherent method-related variability is important. On the basis of these assessments, we chose method (3), i.e., using the fractional cerebellum V_T as V_{ND} to estimate binding potentials. In method (3) the binding potential BP_{ND} in the cerebellum is assumed to have a constant value (i.e., $\alpha - 1$). Thus, the intersubject variability of BP_{ND} in the cerebellum is not taken into account. This approach will be valuable if the specific binding fraction (i.e., BP_{ND}) in the cerebellum is unchanged by diseases and experimental conditions. We also applied the fractional correction to the BP_{ND} estimates from SRTM. The corrected BP_{ND} values correlated very well with those from the MA1 model, but with an underestimation of ~10%.

By correlating BP_F values measured here with KOR B_{max} values measured *in vitro*, we determined an *in vivo* K_D value of 0.028 nmol/L for ^{11}C-LY2795050 in the human brain. We first compared this value with that obtained in rhesus monkeys. An *in vivo* ED_{50} value of 15.6 μg/kg was derived from a ^{11}C-LY2795050 PET study with coinjection of unlabeled LY2795050 in rhesus monkey.[25] We calculated the relationship between the injected LY2795050 dose and plasma concentration from the rhesus monkey data used in the paper by Kim *et al.*[25] To obtain plasma concentration in nmol/L, the measured arterial input functions (Bq/mL) were corrected for protein binding (f_P, 0.018 ± 0.002 in rhesus monkeys) and parent fraction, divided by the specific activity of injected ^{11}C-LY2795050, and then averaged over 40 to 90 minutes after injection of ^{11}C-LY2795050. Using the regression line (plasma concentration (nmol/L) = 0.0065 × injected dose (μg/kg), R^2 = 0.997, Supplementary Figure S4), the *in vivo* ED_{50} of LY2795050 was converted to K_D (0.10 nmol/L).

The *in vivo* K_D estimates of 0.10 nmol/L in rhesus monkeys and of 0.028 nmol/L (0.019 to 0.056 nmol/L using regional B_{max} values from individual *in vitro* studies) in humans for ^{11}C-LY2795050 were smaller than the inhibition coefficient (K_i) of 0.72 nmol/L measured *in vitro* using cloned human KOR. The discrepancy between *in vivo* K_D values and *in vitro* K_i could be attributed to a number of factors. First, the *in vitro* K_i values are usually determined from radioligand competition assays performed at room temperature (22°C), such as in this case for LY2795050, while *in vivo* K_D values are derived from imaging experiments conducted at body temperature (37°C). Temperature sometimes exerts a significant effect on the binding affinities of radioligands, although the direction of changes is not readily predictable (see Elfving *et al*[41]). For example, the *in vitro* K_i of fallypride for the dopamine D_2 receptor in the rat striatum was 0.04 nmol/L at 22°C and 2.03 nmol/L at 37°C, while the *in vivo* K_D derived from imaging experiments with ^{18}F-fallypride in baboons was 0.2 nmol/L.[42] For another D_2 ligand IBF, the *in vivo* K_D (0.081 nmol/L for ^{123}I-IBF) was very similar to the K_i measured *in vitro* at 22°C (0.06 nmol/L) and 37°C (0.10 nmol/L).[43] The benzodiazepine receptor ligand iomazenil is another case in which the *in vivo* K_D (0.54 nmol/L for ^{123}I-iomazenil) derived from imaging experiments was quite similar to the *in vitro* K_i measures either at 22°C (0.35 nmol/L) or at 37°C (0.66 nmol/L).[44]

The uncertainty, or measurement errors in ligand-free fraction in the plasma (f_P), is the second factor that might contribute to the discrepancy between *in vivo* K_D and *in vitro* K_i. f_P values are required in the determination of *in vivo* K_D, as they are used to estimate the free ligand concentrations in the brain. In both rhesus monkeys and humans, ^{11}C-LY2795050 f_P was very small ($< 2\%$), and any small errors in its measurement accuracy will contribute to the uncertainty in the K_D estimate.

In conclusion, we conducted successfully the first *in vivo* evaluation of ^{11}C-LY2795050 in humans. The uptake pattern of ^{11}C-LY2795050 was in good accordance with the known KOR distribution. ^{11}C-LY2795050 displayed favorable kinetic properties and can be used for quantitative PET measurement of KOR in human brain. The 2TC and MA1 models were selected as the best model to describe its kinetics and derive binding parameters. Blocking experiments showed that 150 mg of oral naltrexone provided $> 90\%$ KOR occupancy, and that there was no ideal reference region for ^{11}C-LY2795050 in the human brain. The use of the cerebellum V_T corrected for its small specific binding fraction as V_{ND} was proposed as a method to calculate binding potentials.

DISCLOSURE/CONFLICT OF INTEREST

Johannes Tauscher was employed by Eli Lilly and Company at the time of study.

ACKNOWLEDGMENTS

The authors appreciate the excellent technical assistance of the staff at the Yale University PET Center.

REFERENCES

1 Pfeiffer A, Pasi A, Mehraein P, Herz A. Opiate receptor binding sites in human brain. *Brain Res* 1982; **248**: 87–96.
2 Cross AJ, Hille C, Slater P. Subtraction autoradiography of opiate receptor subtypes in human brain. *Brain Res* 1987; **418**: 343–348.
3 Delay-Goyet P, Zajac JM, Javoy-Agid F, Agid Y, Roques BP. Regional distribution of mu, delta and kappa opioid receptors in human brains from controls and parkinsonian subjects. *Brain Res* 1987; **414**: 8–14.

4 Barg J, Belcheva M, Rowinski J, Ho A, Burke WJ, Chung HD *et al.* Opioid receptor density changes in Alzheimer amygdala and putamen. *Brain Res* 1993; **632**: 209–215.
5 Simonin F, Gaveriaux-Ruff C, Befort K, Matthes H, Lannes B, Micheletti G *et al.* kappa-Opioid receptor in humans: cDNA and genomic cloning, chromosomal assignment, functional expression, pharmacology, and expression pattern in the central nervous system. *Proc Natl Acad Sci USA* 1995; **92**: 7006–7010.
6 Mash DC, Staley JK. D3 dopamine and kappa opioid receptor alterations in human brain of cocaine-overdose victims. *Ann NY Acad Sci* 1999; **877**: 507–522.
7 Shippenberg TS. The dynorphin/kappa opioid receptor system: a new target for the treatment of addiction and affective disorders? *Neuropsychopharmacology* 2009; **34**: 247.
8 de Lanerolle NC, Williamson A, Meredith C, Kim JH, Tabuteau H, Spencer DD *et al.* Dynorphin and the kappa 1 ligand [3H]U69,593 binding in the human epileptogenic hippocampus. *Epilepsy Res* 1997; **28**: 189–205.
9 Loacker S, Sayyah M, Wittmann W, Herzog H, Schwarzer C. Endogenous dynorphin in epileptogenesis and epilepsy: anticonvulsant net effect via kappa opioid receptors. *Brain* 2007; **130**: 1017–1028.
10 Cohen RM, Andreason PJ, Doudet DJ, Carson RE, Sunderland T. Opiate receptor avidity and cerebral blood flow in Alzheimer's disease. *J Neurol Sci* 1997; **148**: 171–180.
11 Mathieu-Kia AM, Fan LQ, Kreek MJ, Simon EJ, Hiller JM. Mu-, delta- and kappa-opioid receptor populations are differentially altered in distinct areas of postmortem brains of Alzheimer's disease patients. *Brain Res* 2001; **893**: 121–134.
12 Mague SD, Pliakas AM, Todtenkopf MS, Tomasiewicz HC, Zhang Y, Stevens WC, Jr. *et al.* Antidepressant-like effects of kappa-opioid receptor antagonists in the forced swim test in rats. *J Pharmacol Exp Ther* 2003; **305**: 323–330.
13 Carlezon WA, Jr., Beguin C, DiNieri JA, Baumann MH, Richards MR, Todtenkopf MS *et al.* Depressive-like effects of the kappa-opioid receptor agonist salvinorin A on behavior and neurochemistry in rats. *J Pharmacol Exp Ther* 2006; **316**: 440–447.
14 Ranganathan M, Schnakenberg A, Skosnik PD, Cohen BM, Pittman B, Sewell RA *et al.* Dose-related behavioral, subjective, endocrine, and psychophysiological effects of the kappa opioid agonist Salvinorin A in humans. *Biol Psychiatry* 2012; **72**: 871–879.
15 Ravert HT, Mathews WB, Musachio JL, Scheffel U, Finley P, Dannals RF. [11C]-methyl 4-[(3,4-dichlorophenyl)acetyl]-3-[(1-pyrrolidinyl)-methyl]-1- piperazinecarboxylate ([11C]GR89696): synthesis and in vivo binding to kappa opiate receptors. *Nucl Med Biol* 1999; **26**: 737–741.
16 Poisnel G, Oueslati F, Dhilly M, Delamare J, Perrio C, Debruyne D *et al.* [11C]-MeJDTic: a novel radioligand for kappa-opioid receptor positron emission tomography imaging. *Nucl Med Biol* 2008; **35**: 561–569.
17 Zheng MQ, Nabulsi N, Kim SJ, Tomasi G, Lin SF, Mitch C *et al.* Synthesis and evaluation of 11C-LY2795050 as a kappa-opioid receptor antagonist radiotracer for PET imaging. *J Nucl Med* 2013; **54**: 455–463.
18 Talbot PS, Narendran R, Butelman ER, Huang Y, Ngo K, Slifstein M *et al.* 11C-GR103545, a radiotracer for imaging kappa-opioid receptors in vivo with PET: synthesis and evaluation in baboons. *J Nucl Med* 2005; **46**: 484–494.
19 Schoultz BW, Hjornevik T, Willoch F, Marton J, Noda A, Murakami Y *et al.* Evaluation of the kappa-opioid receptor-selective tracer [11C]GR103545 in awake rhesus macaques. *Eur J Nucl Med Mol Imaging* 2010; **37**: 1174–1180.
20 Tomasi G, Nabulsi N, Zheng MQ, Weinzimmer D, Ropchan J, Blumberg L *et al.* Determination of in vivo Bmax and Kd for 11C-GR103545, an agonist PET tracer for kappa-opioid receptors: a study in nonhuman primates. *J Nucl Med* 2013; **54**: 600–608.
21 Naganawa M, Jacobsen LK, Zheng MQ, Lin SF, Banerjee A, Byon W *et al.* Evaluation of the agonist PET radioligand [11C]GR103545 to image kappa opioid receptor in humans: Kinetic model selection, test-retest reproducibility and receptor occupancy by the antagonist PF-04455242. *Neuroimage* 2014; **99**: 69–79.
22 Land BB, Bruchas MR, Lemos JC, Xu M, Melief EJ, Chavkin C. The dysphoric component of stress is encoded by activation of the dynorphin kappa-opioid system. *J Neurosci* 2008; **28**: 407–414.
23 Metcalf MD, Coop A. Kappa opioid antagonists: past successes and future prospects. *AAPS J* 2005; **7**: E704–E722.
24 Thomas JB, Atkinson RN, Vinson NA, Catanzaro JL, Perretta CL, Fix SE *et al.* Identification of (3R)-7-hydroxy-N-((1S)-1-[[(3R,4R)-4-(3-hydroxyphenyl)- 3,4-dimethyl-1-piperidinyl]methyl]-2-methylpropyl)-1,2,3,4-tetrahydro- 3-isoquinolinecarboxamide as a novel potent and selective opioid kappa receptor antagonist. *J Med Chem* 2003; **46**: 3127–3137.
25 Kim SJ, Zheng MQ, Nabulsi N, Labaree D, Ropchan J, Najafzadeh S *et al.* Determination of the in vivo selectivity of a new kappa-opioid receptor antagonist PET tracer C-11-LY2795050 in the rhesus monkey. *J Nucl Med* 2013; **54**: 1668–1674.
26 Mitch CH, Quimby SJ, Diaz N, Pedregal C, de la Torre MG, Jimenez A *et al.* Discovery of aminobenzyloxyarylamides as kappa opioid receptor selective antagonists: application to preclinical development of a kappa opioid receptor antagonist receptor occupancy tracer. *J Med Chem* 2011; **54**: 8000–8012.
27 Carson RE, Barker WC, Liow JS, Johnson CA. Design of a motion-compensation OSEM list-mode algorithm for resolution-recovery reconstruction for the HRRT. *IEEE Nucl Sci Symp Conf Rec (2003)* 2003; **5**: 3281–3285.
28 Jin X, Chan C, Mulnix T, Panin V, Casey ME, Liu C *et al.* List-mode reconstruction for the Biograph mCT with physics modeling and event-by-event motion correction. *Phys Med Biol* 2013; **58**: 5567–5591.
29 Hilton J, Yokoi F, Dannals RF, Ravert HT, Szabo Z, Wong DF. Column-switching HPLC for the analysis of plasma in PET imaging studies. *Nucl Med Biol* 2000; **27**: 627–630.
30 Tzourio-Mazoyer N, Landeau B, Papathanassiou D, Crivello F, Etard O, Delcroix N *et al.* Automated anatomical labeling of activations in SPM using a macroscopic anatomical parcellation of the MNI MRI single-subject brain. *Neuroimage* 2002; **15**: 273–289.
31 Holmes CJ, Hoge R, Collins L, Woods R, Toga AW, Evans AC. Enhancement of MR images using registration for signal averaging. *J Comput Assist Tomogr* 1998; **22**: 324–333.
32 Viola P, Wells WM, III. Alignment by maximization of mutual information. *Int J Comput Vis* 1997; **24**: 137–154.
33 Papademetris X, Jackowski M, Rajeevan N, Constable RT, Staib LH. Bioimage suite: an integrated medical image analysis suite. *Insight J* 2005.
34 Innis RB, Cunningham VJ, Delforge J, Fujita M, Gjedde A, Gunn RN *et al.* Consensus nomenclature for in vivo imaging of reversibly binding radioligands. *J Cereb Blood Flow Metab* 2007; **27**: 1533–1539.
35 Ichise M, Toyama H, Innis RB, Carson RE. Strategies to improve neuroreceptor parameter estimation by linear regression analysis. *J Cereb Blood Flow Metab* 2002; **22**: 1271–1281.
36 Frankle WG, Huang Y, Hwang DR, Talbot PS, Slifstein M, Van Heertum R *et al.* Comparative evaluation of serotonin transporter radioligands 11C-DASB and 11C-McN 5652 in healthy humans. *J Nucl Med* 2004; **45**: 682–694.
37 Cunningham VJ, Rabiner EA, Slifstein M, Laruelle M, Gunn RN. Measuring drug occupancy in the absence of a reference region: the Lassen plot re-visited. *J Cereb Blood Flow Metab* 2010; **30**: 46–50.
38 Gunn RN, Murthy V, Catafau AM, Searle G, Bullich S, Slifstein M *et al.* Translational characterization of [11C]GSK931145, a PET ligand for the glycine transporter type 1. *Synapse* 2011; **65**: 1319–1332.
39 Laruelle M, Vanisberg MA, Maloteaux JM. Regional and subcellular localization in human brain of [3H]paroxetine binding, a marker of serotonin uptake sites. *Biol Psychiatry* 1988; **24**: 299–309.
40 Olsson H, Halldin C, Swahn CG, Farde L. Quantification of [11C]FLB 457 binding to extrastriatal dopamine receptors in the human brain. *J Cereb Blood Flow Metab* 1999; **19**: 1164–1173.
41 Elfving B, Bjornholm B, Ebert B, Knudsen GM. Binding characteristics of selective serotonin reuptake inhibitors with relation to emission tomography studies. *Synapse* 2001; **41**: 203–211.
42 Slifstein M, Hwang DR, Huang Y, Guo N, Sudo Y, Narendran R *et al.* In vivo affinity of [18F]fallypride for striatal and extrastriatal dopamine D2 receptors in nonhuman primates. *Psychopharmacology (Berl)* 2004; **175**: 274–286.
43 Laruelle M, al-Tikriti MS, Zea-Ponce Y, Zoghbi SS, Baldwin RM, Charney DS *et al.* In vivo quantification of dopamine D2 receptor parameters in nonhuman primates with [123I]iodobenzofuran and single photon emission computerized tomography. *Eur J Pharmacol* 1994; **263**: 39–51.
44 Laruelle M, Abi-Dargham A, al-Tikriti MS, Baldwin RM, Zea-Ponce Y, Zoghbi SS *et al.* SPECT quantification of [123I]iomazenil binding to benzodiazepine receptors in nonhuman primates: II. Equilibrium analysis of constant infusion experiments and correlation with in vitro parameters. *J Cereb Blood Flow Metab* 1994; **14**: 453–465.

Supplementary Information accompanies the paper on the Journal of Cerebral Blood Flow & Metabolism website (http://www.nature.com/jcbfm)